AO_4 Upside Down: A New Molecular Structure for Supported VO_4 Catalysts

Daphne E. Keller, Frank M. F. de Groot, Diederik C. Koningsberger, and Bert M. Weckhuysen*

Department of Inorganic Chemistry and Catalysis, Debye Institute, Utrecht University, PO Box 80083, 3508 TB Utrecht, The Netherlands

Received: December 1, 2004; In Final Form: March 18, 2005

Vanadium oxide (1 wt %) supported on γ-Al_2O_3 was used to investigate the interface between the catalytically active species and the support oxide. Raman, UV−vis−NIR DRS, ESR, XANES, and EXAFS were used to characterize the sample in great detail. All techniques showed that an isolated VO_4 species was present at the catalyst surface, which implies that no V−O−V moiety is present. Surprisingly, a Raman band was present at 900 cm^{-1}, which is commonly assigned to a V−O−V vibration. This observation contradicts the current literature assignment. To further elucidate on potential other Raman assignments, the exact molecular structure of the VO_4 entity (1 V═O bond of 1.58 Å and 3 V−O bonds of 1.72 Å) together with its position relative to the support O anions and Al cation of the Al_2O_3 support has been investigated with EXAFS. In combination with a structural model of the alumina surface, the arrangement of the support atoms in the proximity of the VO_4 entity could be clarified, leading to a new molecular structure of the interface between VO_4 and Al_2O_3. It was found that VO_4 is anchored to the support oxide surface, with only one V−O support bond instead of three, which is commonly accepted in the literature. The structural model suggested in this paper leaves three possible assignments for the 900 cm^{-1} band: a V−O−Al vibration, a V−O−H vibration, and a V−(O−O) vibration. The pros and cons of these different options will be discussed.

Introduction

Supported vanadium oxide catalysts have been studied extensively in the literature, because of their potential for catalyzing several oxidation reactions, e.g., the oxidation of methanol to formaldehyde and the oxidative dehydrogenation of light alkanes.[1−9] The molecular structure of the vanadium oxide species on several supports; i.e., Al_2O_3, Nb_2O_5, SiO_2, TiO_2, and ZrO_2, has been examined with several techniques, such as Raman, ^{51}V NMR, UV−vis−NIR DRS, and XAFS.[10−15] The molecular structure of the supported vanadium oxide species was found to depend on several parameters, e.g. metal oxide loading, support oxide material, and degree of hydration.[11,15−17] With increasing loading, the vanadium oxide structure changes gradually from monomer to polymer and finally to crystalline V_2O_5.[1,16]

The most widely accepted model for the VO_4 monomeric species in dehydrated samples is the distorted tetrahedral structure with one V═O and three V−O-support bonds. This molecular structure has been proposed for vanadium oxide species on several support oxide materials at low metal oxide loading based mainly on Raman[18−20] and NMR data.[21,22] EXAFS and phosphorescence measurements from Takenaka et al. on a low loaded SiO_2 supported catalyst also report the sole presence of the VO_4 monomer.[19] Anpo et al. have determined the structure of vanadium oxide in a V-silicalite with EXAFS, ESR, and phosphorescence. They also concluded the presence of a monomeric VO_4 species.[23] Though other models, like a di-oxo or octahedrally coordinated species, are suggested as well,[24,25] most researchers agree that a highly distorted mono-oxo monomeric VO_4 species is present on the catalyst surface, i.e., a O_3−V═O species. Although the classical isolated VO_4 model is most widely accepted, the structure of the interface between the VO_4 molecule and the support oxide is not thoroughly investigated.

Eckert and Wachs[21] concluded from NMR data on TiO_2-supported vanadium oxides that a molecular species with more than 2-fold symmetry is present on the surface. Combined with the V═O observed with Raman they conclude that a compound of the $Q^{(3)}$-type is present, i.e., $(Ti-O-)_3V═O$. However, they already mention that there is no suitable reference compound available to check their suggestion for such a structure. Went et al.[26] suggest a similar model on SiO_2 on the basis of Raman measurements. They also observe a very short V═O bond, which resembles the V═O in $VOCl_3$. Since this molecule has C_{3v} symmetry, they conclude that a species with three V−O-support bonds is present on the SiO_2 surface. Anpo et al.[27] state that the $VOCl_3$ molecule used for chemical vapor deposition (CVD) on silica reacts easily with the surface hydroxyl groups to form a $(Si-O)_3V═O$ species. They also mention that the amount of $VOCl_3$ deposited on the SiO_2 surface can be monitored with UV (charge transition of $O^{2-} \rightarrow V^{5+}$) and IR (OH vibration). HCl is formed during the reaction indicating that vanadium is anchored to the surface via V−O−Si bonds. However, the authors did not link the amount of OH groups disappearing nor the amount of HCl formed during reaction and calcination to the amount of vanadium present and thus did not prove unambiguously that the number of V−O-support bonds is three. Although the conclusions drawn by the above-mentioned authors seem to be logical, one has to realize that none of these authors actually delivers conclusive evidence for the way the vanadium oxide is anchored to the support surface.

It has been shown that the support oxide material has a profound influence on the catalytic activity of the supported

* To whom correspondence should be addressed. Tel: +31 30 253 7400. E-mail: b.m.weckhuysen@chem.uu.nl.

10.1021/jp044539l CCC: $30.25
Published on Web 04/27/2005

TABLE 1: Sample Name and Loading Together with Results from Raman and UV−vis Experiments

sample name	sample	loading VO_x/nm^2	UV−vis DRS E_{edge} (eV)	Raman shift cm^{-1}	1030/910 area ratio
1 V−Al	1 wt % V_2O_5/Al_2O_3	0.430	3.19	900 and 1022	1.83
5 V−Al	5 wt % V_2O_5/Al_2O_3	2.15	2.84	908 and 1029	1.55
10 V−Al	10 wt % V_2O_5/Al_2O_3	4.30	2.60	916 and 1034	2.23
15 V−Al	15 wt % V_2O_5/Al_2O_3	6.45	2.42	917 and 1034	1.81

vanadium oxide species. Several examples exist in the literature: the methanol oxidation as reported by Deo et al. and the oxidative dehydrogenation of light alkanes as studied by Khodakov et al.[1,2] The activity could be altered by 3 orders of magnitude by changing the support oxide from SiO_2 to Nb_2O_5.[2] To understand the interaction between the vanadium oxide species and the support oxide, it is important to determine the interfacial structure between those. More in particular, one has to know how many oxygen neighboring atoms are present in the support oxide and where those are situated before an attempt can be made to unravel the influence of the support oxide properties on the catalytic properties of the vanadium oxide. The exact position of support oxygen atoms and support cations with respect to the position of the vanadium atom, has seldom been reported in the literature before. An oxygen atom at a larger distance (2.18 Å) determined with XAFS measurements, has been mentioned by Zhang et al., but they ascribe the larger distance to a partly 5- or 6-fold coordinated vanadium atom.[28] Furthermore, Lin et al. have observed a Ti atom at 2.8 Å with EXAFS for a V_2O_5/TiO_2/MCM-41 catalyst, which might be considered a support cation.[29]

In this paper, we have applied Raman, UV−vis−NIR DRS, ESR, XANES, and EXAFS to determine both the molecular structure of the vanadium oxide present in low loaded vanadium catalyst supported on Al_2O_3 and the structure of the interface between VO_4 and the support oxide. The molecular structure of the VO_4 entity, together with its position relative to the support O anions and Al cation of the Al_2O_3 support has been elucidated on the basis of the acquired spectroscopic data. A structural model of the alumina surface has been used to test and verify the outcome of the spectroscopic results. A new model for the molecular structure of the interface between the isolated VO_4 species and the Al_2O_3 support will be proposed, which clarifies the way the VO_4 unit is anchored to the support oxide. We will show that on the low loaded vanadium oxide catalyst only monomeric species are present. Since the catalyst does not contain any V−O−V moieties, the 900 cm^{-1} Raman band cannot originate from a V−O−V polymeric vibration. Furthermore, three possible assignments, on the basis of our new supported vanadium oxide model, of the 900 cm^{-1} Raman band, i.e., V−O−Al, V−O−H, and V−(O−O) vibrations, will be discussed.

Experimental Section

A. Catalyst Preparation. The Al_2O_3 supported vanadium oxide catalyst was prepared using γ-Al_2O_3 (homemade, S_{BET} = 165 $m^2\ g^{-1}$, V_{pore} = 0.35 mL g^{-1}). The Al_2O_3 support was prepared via the sol−gel method. The series of catalysts was prepared via incipient wetness impregnation with a NH_4VO_3 (Merck, p.a.) solution with oxalic acid (Brocacef, 99.25% pure). Table 1 contains some physicochemical and spectroscopic properties of the catalysts under investigation, together with the catalyst name that will be used throughout this paper. The catalysts were dried at room temperature for one night, one night at 393 K and after this treatment they were calcined at 773 K for 3 h. This resulted in a series of catalysts with a loading range from 0.43 VO_x/nm^2 till 6.45 VO_x/nm^2. For all catalysts the loading is below the monolayer coverage (∼ 10 VO_x/nm^2).[30]

B. Raman, UV−vis−NIR DRS, and ESR Measurements. All catalyst characterization measurements were carried out after dehydration (O_2, 40 mL min^{-1}, 723 K for 3 h) at room temperature. The dehydration pretreatment was carried out in a special cell with quartz window.[31] This cell was used for the Raman and UV−vis measurements and is also equipped with a tube for ESR measurements. The Raman spectrum (exposure time 50 s, 50 accumulations) was collected at room temperature with a Kaiser RXN spectrometer equipped with a 532 nm diode laser. A 5.5″ noncontact objective was used for beam focusing and collection of scattered radiation. As reference substances, solutions containing several vanadium oxide complexes, containing a V−O−V moiety, a monomeric vanadium oxide, or a peroxo group, were measured. The V−O−V containing solution was prepared by dissolving about 0.1 g of NH_4VO_3 in a HNO_3 solution of pH ∼ 2. This resulted in a light yellow colored solution, containing $V_{10}O_{26}(OH)_2^{4-}$ as most abundant species, together with some V_2O_5 precipitate.[32] The monomeric species was prepared by dissolving about 0.001 g of NH_4VO_3 in a NaOH solution of pH ∼ 14. This resulted in a colorless solution containing mostly VO_4^{3-}.[32] The peroxo species was prepared by dissolving NH_4VO_3 in a 5% H_2O_2 solution and acidifying this bright yellow solution with concentrated HNO_3 till pH = 0.5. This resulted in a bright orange-red solution containing $VO(O_2)^+$ with one peroxo group attached to the vanadium atom.[33] The UV−vis−NIR DRS measurements were carried out at room temperature on a Cary 500 UV−vis−NIR equipment from Varian in the range 200−2200 nm. This setup was equipped with a diffuse reflectance accessory, which was set to collect diffuse reflected light only. The scan was made with an averaging time of 0.1 s, data interval of 1 nm, and a scan rate of 600 nm/min. A baseline correction was performed using a white Halon standard. The $F(R\infty)$ was calculated from the absorbance. The edge energy for the charge transfer (CT) bands was calculated via the method described by Delgass et al.[34] The intercept of the straight line at the low-energy rise of a plot of $(F(R\infty)h\nu)^2$ against $h\nu$ was used to determine the edge energy (E_{edge}) for allowed transitions. The ESR measurement on 1 V−Al was performed with an X-band ESP 300 E spectrometer of Bruker, equipped with a TE_{104} cavity. The spectra were collected at 120 K.

C. EXAFS Data Collection. XAFS experiments on 1 V−Al were carried out at E4 in Hasylab (Hamburg, Germany) using a Si (111) monochromator. The measurements were performed in fluorescence mode, using an ion chamber filled with 400 mbar N_2 to determine I_0. The detector used to collect the fluorescent radiation was a 7-element solid state (SiLi) detector. The monochromator was detuned to 80% of the maximum intensity at the V K-edge (5465 eV) to minimize the presence of higher harmonics. The measurement was carried out in an in situ cell with Kapton windows.[35] Data were collected at 77 K after dehydration (723 K for 2 h in 2.5% O_2/He, 100 mL min^{-1}). Four scans were averaged.

D. EXAFS Data Analysis. The EXAFS data analysis was carried out using the XDAP code developed by Vaarkamp et al.[36] The preedge was subtracted using a second order polynomial. The edge position was calibrated by taking the second

derivative of a V-foil spectrum and determining the position of the first inflection point. Normalization was carried out by dividing the data by the height of the absorption 50 eV above the absorption edge. The background was subtracted employing cubic spline routines with a continuously adjustable smooth parameter.[37] This led to the normalized oscillatory part of the XAFS data, for which all of the contributions to the spectrum, including the AXAFS, were maximized.[37]

The EXAFS data-analysis program XDAP allows one to perform multiple-shell fitting in R-space by minimizing the residuals between both the absolute and the imaginary part of the Fourier transforms of the data and the fit. The absolute part of the FT is determined mainly by the number of neighbors (N) and the disorder (Debye−Waller factor; $\Delta\sigma^2$) of the different coordination shells. The imaginary part can be used to accurately determine the interatomic distances for the different absorber-scatterer pairs contributing to the EXAFS spectrum (R). The imaginary part can also be very useful in the discovery of unknown contributions. R-space fitting has important advantages compared to the usually applied fitting in k space and is extensively discussed in a paper by Koningsberger et al.[37] The variances of the magnitude and imaginary part of the Fourier transforms of fit and data were calculated according to

$$\text{variance} = \frac{\int [\text{FT}\,(k^n\chi_{\text{model}}) - \text{FT}(k^n\chi_{\text{exp}})]^2\,\text{d}R}{\int [\text{FT}(k^n\chi_{\text{exp}})]^2\,\text{d}R} \times 100 \tag{1}$$

The data discussed in this paper were analyzed using a multiple shell R-space fit with k^1 weighting, $\Delta k = 2.5-11$ Å^{-1} and $\Delta R = 0.7-5.0$ Å. The validity of the fit was checked in all k weightings (k^n with $n = 0$, 1, 2, and 3). The fit-range resulted in the number of independent parameters (N_{ind}) that may be optimized, according to the Nyquist theorem[38]

$$N_{\text{ind}} = \frac{2\Delta R \Delta k}{\pi} + 2 \qquad \text{to be } 25.3$$

The difference file technique was applied together with phase-corrected Fourier transforms to resolve the different contributions in the EXAFS data.[37] If the experimental spectrum is composed of different contributions then

$$\text{exp. data} = \sum_{i=1}^{N} (\text{fit})_i \tag{2}$$

whereby $(\text{fit})_i$ represents the fitted contribution of coordination shell i. For each individual contribution, the following equation should then logically be valid:

$$(\text{fit})_j = \text{exp. data} - \sum_{i=1 \text{ and } i\neq j}^{N} (\text{Fit})_i \tag{3}$$

The right-hand side of eq 3 is further denoted as the difference file of shell j. A good fit is obtained only if the total fit and each individual contributing coordination shell describe correctly the experimental EXAFS and the difference file, respectively. In this way not only the total EXAFS fit, but also the individual fits of all separate contributions can be determined reliably. In this study, the statistical significance of a contribution has been checked by a comparison of the amplitude of $(\text{fit})_j$ with the noise level present in the experimental data.

Data for the V−O phase shift and backscattering amplitude were obtained from calculations using the FEFF8 code.[39,40] The theoretical reference was calibrated on the experimental EXAFS data of Na_3VO_4 using an R-space fit. The fit parameters for the experimental Na_3VO_4 EXAFS data using the optimal theoretical reference data are presented in Table 2a. Table 2b gives the crystallographic data[41] and the input parameters for FEFF 8 used to create the theoretical EXAFS reference. The input parameters of the FEFF8 code were adjusted until the experimental reference was fitted with $\Delta\sigma^2 = 0$, $\Delta E_0 = 0$, with the resulting distance and the coordination number the same as the crystallographic data. The parameters used to calculate the V−Al and V−V theoretical reference are also given in Table 2b. Suitable experimental reference compounds were not available for calibration purposes. The scattering potentials are calculated by overlapping free atom electron densities within the muffin-tin approximation. A Hedin−Lundqvist[42] potential was used to calculate the phase shift and the backscattering amplitude. The reference spectrum was measured at room temperature, the sample was measured at liquid nitrogen temperature. This means that, besides a difference in structural disorder, a temperature effect has to be included in the difference in Debye−Waller factor ($\Delta\sigma^2$) between sample and reference as obtained in the EXAFS data-analysis.

TABLE 2: (a) Fit Parameters for the *R*-Space Fit of Na_3VO_4 and (b) Crystallographic Data and the Input Parameters for FEFF 8 Used to Create the Theoretical Reference Files for the V−O, V−Al, and V−V Scatterer Pair

a

Fourier transform		k	R				variance	
Δk	ΔR	weighting	N	(Å)	$\Delta\sigma^2$	E_0	Im	Abs
2.5−10	0.8−1.7	k^2	3.9	1.71	0	0	0.099621	0.0751

b

atom pair	ref. comp.	ref	N	R (Å)	σ^2	V_r (eV)	V_i (eV)	S_0^2
V−O	Na_3VO_4	40	4	1.696	0.004	−2.2	1	0.84
V−Al			1	3.28	0	0	1	0.84
V−V			1	3.30	0	0	1	0.84

E. Structural Model for γ-Al_2O_3. The structural model of the VO_4 unit on the γ-Al_2O_3 surface was produced using the CERIUS 2 molecular modeling software.[43] The γ-Al_2O_3 crystal was build up from X-ray diffraction data obtained and interpreted by Zhou et al.[44] Subsequently, this crystal was cut along the (110) plane to expose the preferentially exposed surface, i.e., the D layer according to the LEIS measurements performed by Stobbe-Kreemers et al.[45]

To create a structural model for supported vanadium oxide, a VO_4 molecule was attached to the Al_2O_3 surface. The distances of the $V{=}O_{(1)}$ and $V-O_{(2)}$ coordinations of the VO_4 unit as found in the EXAFS analysis were used as input parameters for the CERIUS 2 molecular modeling program. The coordination number and distance of the $V-O_{(3)}$ and $V-Al_{(4)}$ higher coordination shells, as found in the EXAFS analysis, were taken as structural constraints. Rotation of the VO_4 unit around the $Al_{support}-O_{(2)}$ bond and bending of the $V-O_{(2)}-Al_{support}$ bond were the only performed operations to find a configuration that fitted the EXAFS data. The atoms belonging to the Al_2O_3 support were kept fixed at all times.

Results

A. Raman, UV−vis−NIR DRS, and ESR Measurements. The Raman spectrum for 1 V−Al after dehydration as presented in Figure 1a shows a vibration at 1022 cm^{-1}, which can be

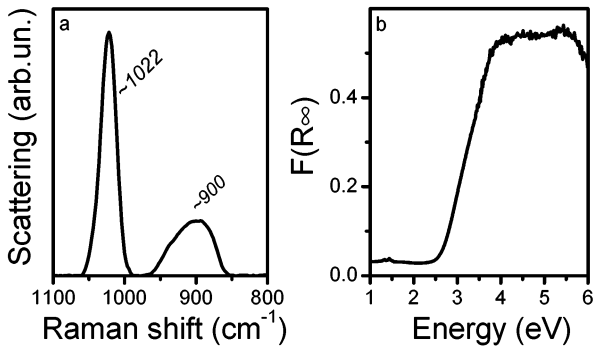

Figure 1. (a) Raman spectrum of 1V−Al; (b) UV−vis DRS spectrum of 1V−Al. Spectra were obtained under dehydrated conditions at room temperature.

assigned to a vanadium oxide species. For all other catalysts discussed in this paper, the observed Raman bands are listed in Table 1. According to the literature, the 1022 cm^{-1} band is due to the V═O vibration of an isolated VO_4 species on the surface of the catalyst.[12,46] A second band is observed at ∼900 cm^{-1}, usually this band is assigned to polymeric vanadium oxide species. However, recently the assignment of the ∼900 cm^{-1} band to polymeric species is under discussion. Magg et al. proposed that this band is due to a V−O-support vibration of a monomeric VO_4 species[47] and our group showed via theoretical calculations on an alumina supported system that the ∼900 cm^{-1} band can be assigned to the stretching vibration of a peroxo O−O species attached to an isolated vanadium oxide species.[48] In the original vibrational spectrum, no bands could be assigned to either polymeric or crystalline vanadium oxide[46,49−51] or Al_2O_3.[18,52] All other vibrations were due to the glass from the sample cell. For clarity, these glass bands were subtracted from the original spectrum, leading to Figure 1a.

The UV−vis−NIR DRS spectrum measured on the 1 V−Al catalyst is shown in Figure 1b. The UV−vis edge energy is influenced by the polymerization degree of the vanadium cations, changes in the coordination geometry, and changes in the second coordination shell around the vanadium cations. The value of the edge-energy is 3.19 eV and lies in the isolated VO_4 region (≥2.8 eV).[15] Table 1 shows that with increasing loading the UV−vis edge energy decreases, indicating a higher polymerization degree for the higher loaded vanadium oxide catalysts. The CT band for the 1 V−Al sample around 3.8−5.5 eV indicates that the vanadium in the VO_4 cluster was present as V^{5+}. D−d transitions, which are typical for reduced vanadium species, are not observed. The absence of V^{4+} in the 1 V−Al sample, as indicated by the UV−vis−NIR DRS measurement, was further checked with ESR measurements. The ESR data showed no significant amount of vanadium (IV) present in this sample (<1%).

The results of all three techniques as given above point to the presence of an isolated VO_4 species in the 5+ oxidation state in the low loaded 1 V−Al sample. Furthermore, it is very unlikely that other vanadium oxide species are present on the surface of the γ-Al_2O_3 support at the low vanadium surface coverage (0.43 VO_x/nm^2). The low loaded 1-VAl catalyst was further used for a detailed EXAFS analysis described in this paper.

B. X-ray Absorption Near Edge Data. The preedge and XANES region are shown in Figure 2. The large preedge peak is due to a 1s−3d transition and is allowed to the presence of a noncentro symmetric species such as a tetrahedron. According to Wong et al., the height of the preedge peak compared to the height of the edge-jump allows us to determine the symmetry

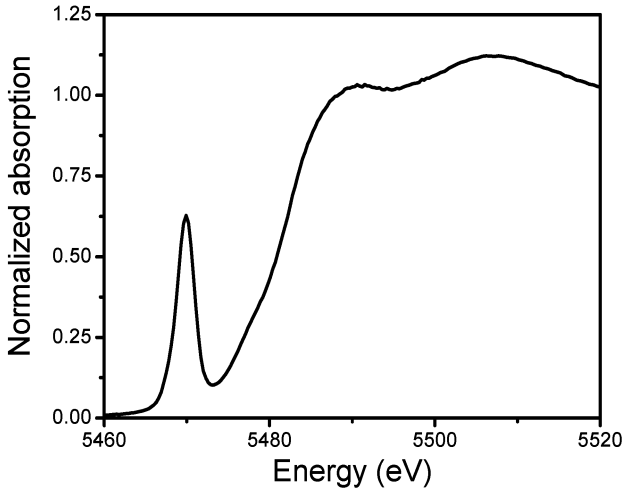

Figure 2. XANES region of the XAFS spectrum for the dehydrated 1 V−Al sample, with a clear preedge peak, measured at 77 K under dehydrated conditions.

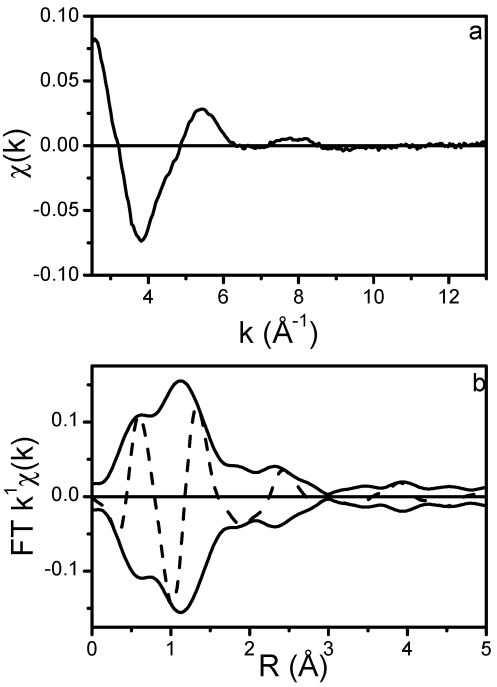

Figure 3. (a) Experimental EXAFS data ($\chi(k)$) of 1V−Al, measured at 77 K under dehydrated conditions; (b) k^1 weighted Fourier transform (Δk = 2.5−11 $Å^{-1}$, ΔR = 0.7−5.0 Å) of the experimental $\chi(k)$ for 1V−Al, absolute (—) and imaginary (- - -) part.

of the species found on the surface.[53] For a perfect tetrahedron, this value is 0.8−1.0. The value observed here is 0.673 indicating that the structure of the vanadium oxide species resembles a distorted tetrahedron. This is fully consistent with the results obtained from Raman and UV−vis. The distance between the preedge peak and the edge is a measure of the oxidation state of vanadium in the sample. For the 1V−Al sample, a value of 12.5 eV was observed. Literature values for tetrahedral V(V) species lie between 12.4 and 12.8 eV. For a square pyramidal V(V) (V_2O_5), the $E_{edge} - E_{pre-edge}$ value is 9.5 eV.[53] This strongly points toward the presence of a tetrahedrally coordinated V^{5+} species.

C. EXAFS Analysis. The EXAFS spectrum as obtained after background subtraction and normalization is given in Figure 3a. The signal-to-noise ratio is 53, with the amplitude determined between k = 2.5 and 4 $Å^{-1}$ and the noise level between k = 11

TABLE 3: Structural Parameters for the Fit of 1V−Al, Obtained Using Model I[a]

	N	R (Å)	$\Delta\sigma^2$	ΔE_0 (eV)
V═$O_{(1)}$	1	1.58	−0.00500	1.75
V−$O_{(2)}$	3	1.72	0.00069	7.73
V- - -$O_{(3)}$	1	2.29	0.02300	−3.28
V- - -$Al_{(4)}$	1	3.09	0.01880	7.53
V- - -$O_{(5)}$	2	3.50	0.01190	−1.13
V- - -$O_{(6)}$	2	4.32	0.01200	−3.40

[a] N = coordination number; R = distance in Å; $\Delta\sigma^2$ = Debye−Waller factor, i.e., disorder; E_0 = inner potential (eV).

TABLE 4: Structural Parameters for the Fit of 1V−Al, Obtained Using Model II[a]

	N	R (Å)	$\Delta\sigma^2$	ΔE_0 (eV)
V═$O_{(1)}$	1	1.58	−0.00500	1.75
V−$O_{(2)}$	3	1.72	0.00069	7.73
V- - -$O_{(3)}$	1	2.41	0.02300	−9.37
V- - -$V_{(4)}$	1	3.21	0.01378	20.29
V- - -$O_{(5)}$	4.2	3.83	0.00703	16.48

[a] N = coordination number; R = distance in Å; $\Delta\sigma^2$ = Debye−Waller factor, i.e., disorder; E_0 = inner potential (eV).

and 13 $Å^{-1}$. The corresponding Fourier transform (k^1, Δk = 2.5−11 $Å^{-1}$) is plotted in Figure 3b. Multiple shell fitting in R-space was applied to determine all of the different absorber-backscatterer pairs contributing to the FT between $0.7 < R < 5$ Å. The fit was evaluated in all weightings (k^n with n = 0, 1, 2, and 3) to unravel anti-phase behavior, which can easily lead to the nondetection of a particular contribution when only one particular weighting is used.[37,54,55] All contributions were fitted simultaneously in R space with at the same time an inspection of the FT of the difference file and calculated fit of each individual contribution.

The main peak in the Fourier transform of the raw data (Figure 3b) represent the VO_4 unit. A good fit in R-space could be obtained for $0.7 < R < 2$ Å with one oxygen atom at a small distance (1.58 Å) (V═O bond) and three oxygen atoms at a larger distance (1.72 Å) (V−O bond). The EXAFS coordination parameters of the first two V−O shells are given in Tables 3 and 4. The agreement between the FT of the fit and the data can be seen in Figure 4a. The deviations for values of R lower than 0.7 Å are caused by the presence of the atomic XAFS (AXAFS) contribution in the FT, for which the background subtraction was optimized. It can also be seen in Figure 4a that for values of R higher than 2 Å differences exist between the Fourier transforms of the fit and the data. This can be more clearly observed in Figure 4b, which shows the R region of the higher coordination shells using an expanded scale with a smaller FT k range to minimize the influence of the noise.

Two different geometrical models were explored to describe the higher coordination shells. It is logical to assume that the VO_4 species must have at least one chemical bond with the surface plane of the Al_2O_3 support. Also the detection with EXAFS of the presence of nonbonding anions or cations cannot be excluded.

In model I, the higher coordination shells were fitted with O and Al atoms of the support. One V−$O_{(3)}$ at 2.29 Å and one V−$Al_{(4)}$ at 3.09 Å coordination could be detected. Subsequently, the values of the V═$O_{(1)}$ and V−$O_{(2)}$ coordinations of the VO_4 unit as found in the EXAFS analysis were used as input parameters for the CERIUS 2 molecular modeling program. The vanadium atom from the VO_4 species is positioned above the support surface in such a way that there is only one oxygen neighbor in the third shell and one aluminum neighbor in the fourth shell using the V−$O_{(3)}$ and V−$Al_{(4)}$ higher coordination

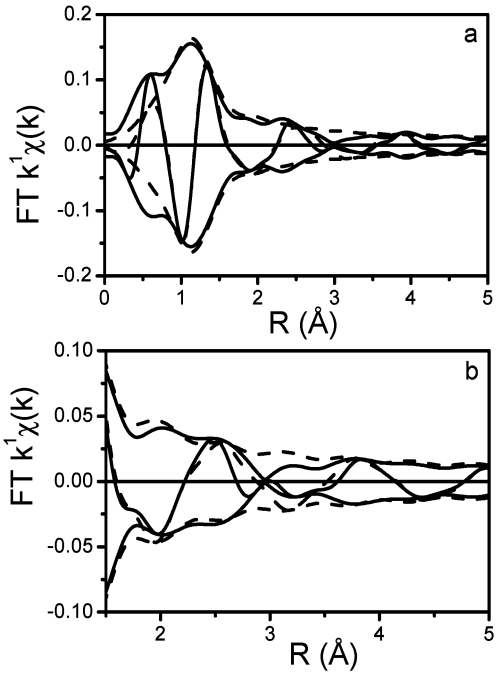

Figure 4. (a) k^1 weighted Fourier transform (Δk = 2.5−11 $Å^{-1}$) of the experimental $\chi(k)$ (—) for 1V−Al and the calculated fit (- - -) in R space (ΔR = 0.7−5.0 Å) for the first two shells. (b) k^1 weighted Fourier transform (Δk = 2.5−8 $Å^{-1}$) of the experimental $\chi(k)$ (—) for 1V−Al and the calculated fit (- - -) in R space (ΔR = 0.7−5.0 Å) for the first two shells. At higher R values, the fit deviates substantially from the experimental data. The first two shells represent the VO_4 unit on the support-surface. Obviously more shells are needed to complete the fit.

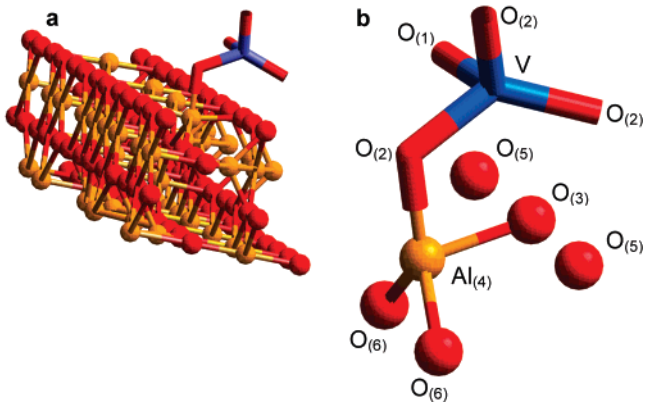

Figure 5. (a) New model of a VO_4 species on the D-layer of the (110) surface of a γ-Al_2O_3 crystal. The VO_4 species is attached to a support aluminum ($Al_{(4)}$, light gray sphere). The support oxygens ($O_{(3)}$, $O_{(5)}$, and $O_{(6)}$) are depicted as dark gray spheres. $O_{(1)}$ and $O_{(2)}$ from the V═O and V−O bonds are depicted as dark gray rods. The vanadium scatterer atom itself is depicted as a light gray tetrahedral rod structure. (b) A detail of the model depicting all atoms fitted with EXAFS for model I.

shells as found in the EXAFS analysis as structural constraints. A structural model satisfying the conditions outlined above is shown in Figure 5a.

Rotation of the VO_4 unit around the $Al_{support}$−$O_{(2)}$ bond and bending of the V−$O_{(2)}$−$Al_{support}$ bond were the only performed operations to find a configuration, in which a V−O distance of 2.29 Å and a V−Al of 2.93 Å were observed as listed in Table 5. These distances are very close to the distances as observed with EXAFS. The geometrical model as based upon the results of EXAFS and structural modeling of the alumina surface is further used to optimize the analysis of the higher coordination

TABLE 5: Interatomic Distances for the γ-Al_2O_3 Supported VO_4 Molecule, Obtained from the Model Produced with CERIUS 2

atom pair	shell	distance (Å)		coordination no.
V═O	1	1.58		1
V−O	2	1.72		3
V- - -O	3	2.29		1
V- - -Al	4	2.93		1
V- - -O[a]	5	3.57	3.65	2
V- - -O[a]	6	4.26	4.30	2

[a] The two distances found for this shell cannot be separated with EXAFS.

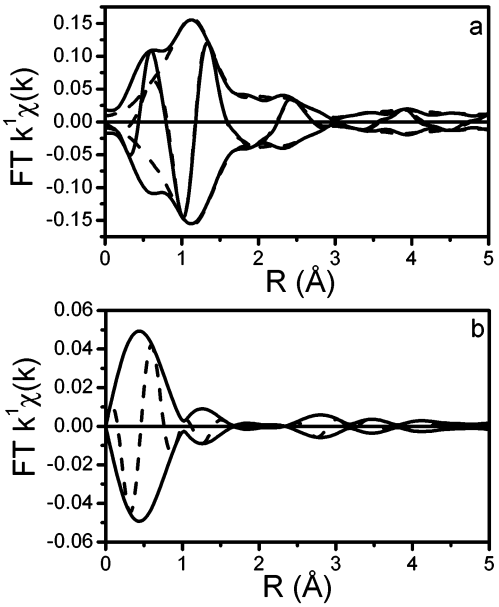

Figure 6. (a) k^1 weighted Fourier transform ($\Delta k = 2.5-11$ Å^{-1}) of the experimental $\chi(k)$ (—) for 1V−Al, the calculated fit (- - -) in R space ($\Delta R = 0.7-5.0$ Å) for Model I; (b) k^1 weighted Fourier Transform of the residue (raw-total fit) $\Delta k = 2.5-8$ Å^{-1}, containing the AXAFS at low R value and nonseparable higher shell contributions. The residue indicates the absence of nonfitted contributions for model I.

shells. According to the CERIUS 2 model, two more V−O shells should be observed in the EXAFS analysis. In Table 3, the resulting EXAFS coordination parameters are given for all six coordination shells. All atoms shown in Figure 5b were observed with EXAFS, at the approximate distances determined from the model.

A comparison of Figures 4a and 6a makes clear that the addition of the higher shells leads to a significantly better fit in the R range $0.7 < R < 5$ Å. The FT of the residue (raw data − total fit) in Figure 6b shows the AXAFS contribution peaking around 0.5 Å. Moreover, no other higher shell contributions are visible in the FT of the residue, meaning that all contributions have been fitted.

The analysis of the higher shells has been depicted in more detail in Figure 7a−c. In Figure 7a, the FT of the difference file (raw − $O_{(1)}$ − $O_{(2)}$) and the FT of the EXAFS function representing the fit of the higher coordination shells ($O_{(3)}$ + $Al_{(4)}$ + $O_{(5)}$ + $O_{(6)}$) are shown. To judge the quality of the fit, one has to realize that the scale of the FT in Figure 7a is about 10% of the full scale of the FT of the total EXAFS (Figure 6a). Figure 7b gives the magnitude of the FT's of the individual coordination shells, showing the peak position of each contribution. Figure 7c makes clear that the 3rd and 5th shells are out of phase with the 4th and 6th shells, respectively. This means that strong interference effects are present and that these

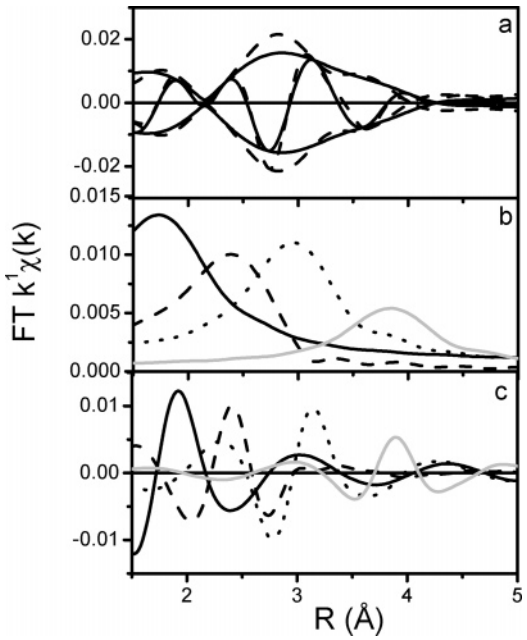

Figure 7. (a) Difference file for raw $O_{(1)}-O_{(2)}$ (—) and $O_{(3)}$ + $Al_{(4)}$ + $O_{(5)}$ + $O_{(6)}$ (- - -) from EXAFS of 1V−Al for model I. (b) Magnitude of the Fourier transform for the separate shells: $O_{(3)}$ (—), $Al_{(4)}$ (- - -), $O_{(5)}$ (···), and $O_{(6)}$ (gray line). (c) The imaginary part of the Fourier transform for the separate shells: $O_{(3)}$ (—), $Al_{(4)}$ (- - -), $O_{(5)}$ (···), and $O_{(6)}$ (gray line). The 3rd and 5th shells are out of phase with the 4th and 6th shells, respectively. This means that these contributions will partly cancel out in the total EXAFS fit.

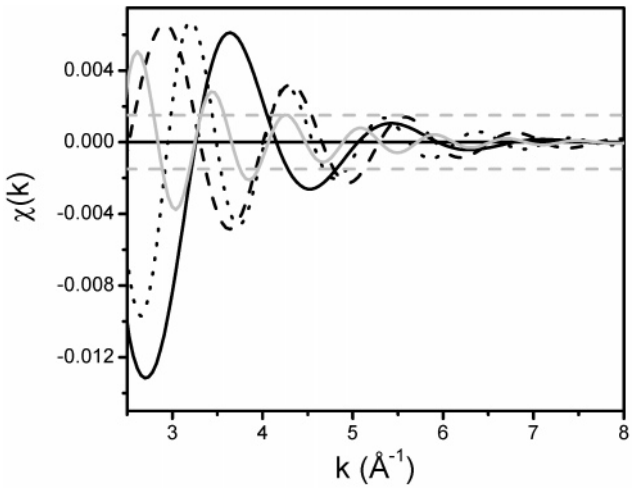

Figure 8. k^0 weighted χ function of the separate higher shells, $O_{(3)}$ (—), $Al_{(4)}$ (- - -), $O_{(5)}$ (···), and $O_{(6)}$ (gray line), together with the noise level.

contributions partly cancel out in the total EXAFS fit, again stressing the fact that the fit should be checked with multiple k-weightings in order to unravel anti-phase behavior.

The statistical significance of the higher shells originating for the support can be evaluated from Figure 8, showing the individual EXAFS functions of the higher shells together with the maximum peak to peak noise level of ±0.0015. All higher shell contributions are well above the noise level at low values of k.

A second model has also been explored (model II). Although the loading of our catalyst is very low, it is still possible that we might observe a vanadium scatterer in the higher shells. This would imply the presence of oligomeric or polymeric species or even two monomeric species close together. The fit parameters used for the total fit of model II are listed in Table 4 and

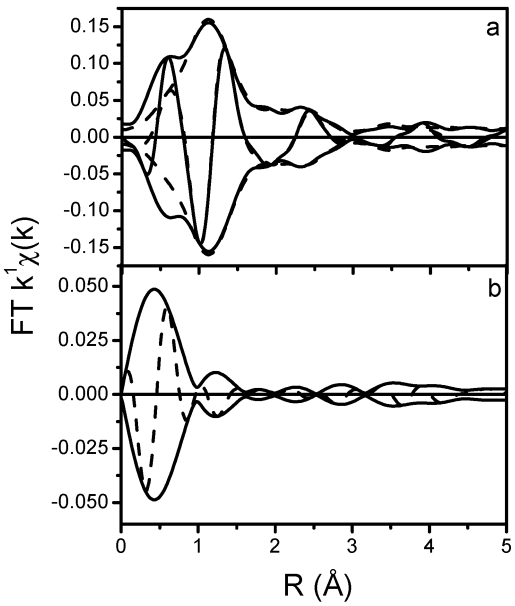

Figure 9. (a) k^1 weighted Fourier transform ($\Delta k = 2.5-11$ Å^{-1}) of the experimental $\chi(k)$ (—) for 1V−Al and the calculated fit (- - -) in R space ($\Delta R = 0.7-5.0$ Å) for model II; (b) k^1 weighted Fourier transform of the residue (raw-total fit) $\Delta k = 2.5-8$ Å^{-1}, containing the AXAFS at low R value and nonseparable higher shell contributions. The residue indicates the absence of nonfitted contribution for model II.

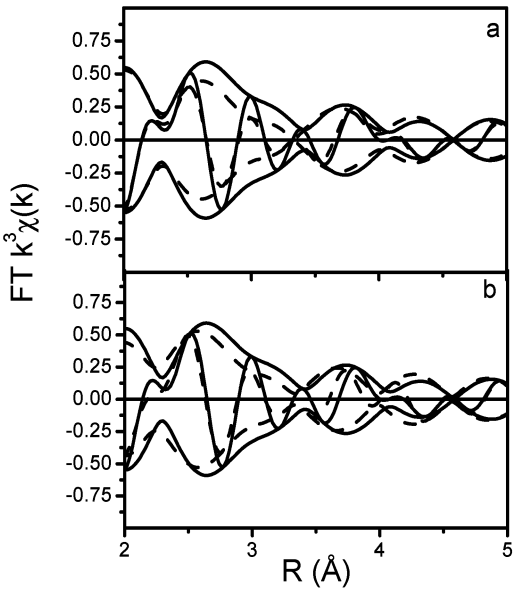

Figure 10. k^3 weighted Fourier transform ($\Delta k = 2.5-8$ Å^{-1}) of the experimental $\chi(k)$ (—) for 1V−Al, the calculated fit (- - -) in R space ($\Delta R = 0.7-5.0$ Å); (a) for model I; (b) for model II; The nodes around $R = 3.5$ Å are better for model I than for model II indicating that model I is a better fit for our EXAFS data; i.e., the scatterer in the fourth shell is an aluminum atom.

the FT of the total fit is displayed in Figure 9a. The Fourier transform of the residue (raw data − total fit) is given in Figure 9b, indicating that no contributions were left unfitted between $0.7 < R < 5$ Å. The only features left in the residue are due to the AXAFS contribution at lower R value and nonseparable higher shell contributions. The details of the FT of the fit of the higher coordination shells are illustrated in Figure 10a−c.

Discussion

Presence of an Isolated VO_4 Molecule. *A. XANES, UV−vis−NIR, and ESR.* The height of the preedge peak compared to the height of the edge-jump allows us to determine the symmetry of the vanadium oxide species found on the support oxide surface.[53] For a perfect tetrahedron this value is 0.8−1.0. The value observed here is 0.673 indicating that the molecular structure of the vanadium oxide species resembles a distorted tetrahedron. The energy difference between the edge and preedge from the XAFS experiment ($E_{edge} - E_{pre-edge} = 12.5$ eV) strongly points to tetrahedrally coordinated V(V) species. Literature values for tetrahedrally coordinated vanadium 5+ species lie between 12.4 and 12.8 eV. For V_2O_5, in which the vanadium atoms have a square pyramidal coordination, this value is 9.5 eV. For compounds with a lower oxidation state the $E_{edge} - E_{pre-edge}$ value rapidly decreases.[53]

The presence of an isolated VO_4 molecule on the Al_2O_3 surface is further supported by the UV−vis edge energy. The value of the edge-energy is 3.19 eV and lies in the isolated VO_4 region (≥2.8 eV).[15] The CT band around 3.8−5.5 eV indicates that the vanadium in the VO_4 cluster was present as V^{5+}. D−d transitions, which are typical for reduced vanadium species, are not observed. The absence of V^{4+} was confirmed with ESR measurements. No significant amount of vanadium (IV) was present in the sample (<1%). So, UV−vis−NIR DRS, ESR, and XANES all point in the direction of an isolated VO_4 species with the vanadium in the 5+ oxidation state.

B. EXAFS Analysis. One could argue whether the fourth shell is due to a support cation or a neighboring V scatterer. A neighboring V scatterer is expected to be present, when dimeric, polymeric, or crystalline vanadium oxide species are present on the catalyst surface or in the case that monomeric species are placed very close together at the surface. If two monomers were close together, the distance between two "neighboring" vanadium atoms would be 6.6 Å for the classical model with three support bonds. This distance is so large that it would not be observed with EXAFS. For a polymeric species, the V−V distance would be 3.8 Å. In the EXAFS fit, we find a maximum distance for the 4th shell of 3.2 Å. A di- or polymeric species would be dispersed on the support, implying that the vanadium atoms are in close proximity of the support Al cations. If a V−V scatterer pair would exist in the sample, we would still expect that we need a contribution from the support Al cations to complete the EXAFS fit. Although model II (assuming a V scatterer to be present within the coordination sphere of V) results in a good fit, no support contributions were needed, which makes model II less acceptable. As is obvious from the FT of the residue of model II EXAFS shown in Figure 9b, no contributions were left unfit. Though the variances in imaginary and absolute part are almost the same, indicating that the quality of the fit is the same for both models, one can see from Figure 10 that the nodes around $R = 3.5$ Å are much better described by model I than by model II. Furthermore, the E_0 value for the fourth shell in model II (the V scatterer) has an unacceptable high value, indicating that vanadium is not the right choice to fit the 4th shell. This means that the presence of a vanadium atom as a neighboring atom is unlikely.

The EXAFS analysis, together with the results from UV−vis−NIR, ESR, and the low catalyst loading, shows that the presence of a vanadium oxide species on the support surface with a V−O−V moiety is highly unlikely. The most plausible structure would be a monomeric distorted tetrahedral VO_4 molecule.

Structural Model for a VO_4 Species on an Al_2O_3 Support. The higher shells observed in the FT of the EXAFS data can give precise information on the position of the support oxygens and cation with respect to the vanadium atom. Zhang et al. report

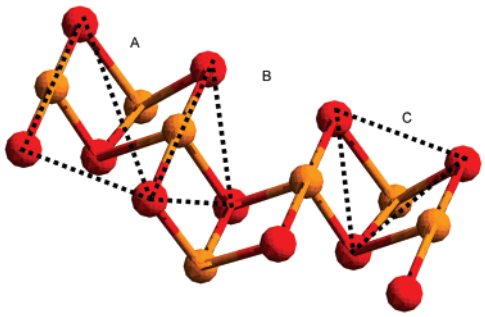

Figure 11. Schematic representation of the different surface anchoring sites for the pyramid model on the 110-plane of γ-Al_2O_3. The dotted lines illustrate the triangular sites A, B, and C, needed for the anchoring of the classical pyramid model.

TABLE 6: Comparison of the Distances Obtained from the EXAFS Analysis with the Distances for the Classical Pyramid Model on the Three Possible Anchoring Sites A, B, and C

	EXAFS results	site A			site B			site C		
scatterer pair	distance (Å)	distance (Å)			distance (Å)			distance (Å)		
V−$O_{(2)}$	1.72	2.39	2.82	2.85	2.13	2.21	2.56	1.78	1.81	1.75
V- - -$O_{(3)}$	2.29									
V- - -Al		1.93	2.31		1.46	1.86		1.59	1.64	
V- - -Al								2.88		
V- - -$Al_{(4)}$	3.09				3.02			3.19		

the presence of a higher oxygen shell at 2.18 Å.[28] They ascribe this contribution to a partly 5- or 6-fold coordination of the vanadium atom. Although the distance is in the same range as for our third shell, the coordination number does not suggest that this is a support oxygen. Only 0.3 support oxygen per vanadium atom would suggest that approximately 33% of the vanadium atoms is bound to the surface via one V−O-support bond. This seems highly unlikely, since it would also imply that 66% of the vanadium atoms is not bound to the surface at all. Furthermore, Lin et al. observed a Ti cation at 2.8 Å, which can be considered a support cation.[29] The support used in their study is TiO_2/MCM-41. One can only conclude that the vanadium atom is in close proximity of the titanium atom supported on a MCM-41 solid. Although atoms from the support oxide might not have been observed for the first time, we have been able to observe several support atoms until a fairly large distance.

In Figure 11, the three possible anchoring sites for the classical pyramid model on a 110-surface of γ-Al_2O_3 are depicted, and Table 6 lists the distances to neighboring atoms as obtained from EXAFS and from the structural model for sites A, B, and C. For sites A and B, the second shell V−$O_{support}$ distances were much too long for a tetrahedrally coordinated vanadium oxide species. A major reorganization of the alumina surface would be required to make the pyramid model fit on these sites. On sites A and B, it would be highly unlikely for the vanadium oxide species to anchor with three V−O bonds to the support. For site C, the V−$O_{support}$ distances were in the range of the values obtained from the EXAFS analysis. In this case, only a small rearrangement of the surface would be required to make the V−O distances for the pyramid model match with the data obtained from the EXAFS analysis. However, the oxygen atom at 2.29 Å observed with EXAFS in the third shell was not found in the structural model of the pyramid structure on site C. The third shell oxygen atom was also not found for site A nor site B. Furthermore, for all three anchoring sites, aluminum atoms were found in the structural model at very short distances (R = 1.46−2.31 Å) from the vanadium atom. These short V- - -Al distances were not observed with EXAFS and neither was the V- - -Al distance in model C of 2.88 Å. Although sites without these nearby aluminum atoms can be found on the γ-Al_2O_3 surface, it is absolutely not trivial to find an anchoring site suitable for the pyramid model that fits the data obtained from EXAFS.[46]

Taking the tetrahedron configuration as independent input, 6 independent parameters are needed for the first two coordination shells. This means that for the total fit of model I 22 independent parameters are needed. The occurrence of a contribution to the total EXAFS spectrum at R = 4.35 Å for model I justifies the use of a large R range. According to the Nyquist theorem 25.3 independent parameters are allowed in the EXAFS fitting process.[38] This implies that the number of free EXAFS parameters used in the fitting process does not exceed the maximum number of allowed independent fit parameters. Figure 8 makes clear that the EXAFS amplitudes of the coordination shells arising from the interface between the VO_4 species and the support are well above the noise level at low values of k. This shows that model I describes an interfacial structure that is statistically allowed in the EXAFS data-analysis.

We were able to link the EXAFS results from model I to a reasonable structural model for a VO_4-unit on a γ-Al_2O_3 surface. As shown in detail in the results section and in the discussion above, an iterative process using the results of the EXAFS analysis together with a structural model rules out an interfacial structure with three oxygen bonds to the support. Instead, a supported low loaded vanadium oxide catalyst consists of one single V−O-support bond, one double V═O bond and two single V−O bonds. The fact that we can present a reasonable structural model for model I, which fits the EXAFS and all other characterization data, we conclude that the structure of the interface between the VO_4 molecule and the support is described by model I. It can be seen in Tables 3 and 5 that the higher shell coordinations obtained from the EXAFS analysis and the structural model are very close. Figure 5 gives a graphical interpretation of the proposed model (model I).

This umbrella model is in accordance with the one presented in a previous paper from our group. Temperature-dependent Raman measurements in combination with DFT calculations showed that the classical pyramid structure could not explain the Raman spectra of the catalyst, whereas the umbrella model mimicked the experimental data. A structure similar to the umbrella structure has been proposed for Rhenium oxide.[48] Rice and Scott have shown quantitatively for $VOCl_3$ adsorbed on SiO_2 that only one bond to the surface is formed, regardless of the amount of OH groups present on the surface.[56,57] Furthermore, Deguns et al. showed with EXAFS analysis that $VOCl_3$ absorbed on a SiO_2 surface results in a (SiO)$VOCl_2$ compound. They observed V═O (1.58 Å) and V−O (1.78 Å) distances similar to the distances reported in this paper for the Al_2O_3 supported vanadium oxide species.[58]

Assignment of the Raman 900−920 cm^{-1} Vibration. Since alumina itself does not have any Raman bands between 100 and 1100 cm^{-1},[18,52] and the bands for the glass sample cell are found at different positions,[59] the band at ∼900 cm^{-1} has to come from the vanadium oxide species present on the surface. Previously, the Raman band at 900−920 cm^{-1} was assigned to polymeric species.[60] Recently, the assignment of this band is under discussion[47,48] and will be further discussed in this paper.

UV−vis edge energy results presented in Table 1 showed that the polymerization degree of the vanadium oxide species

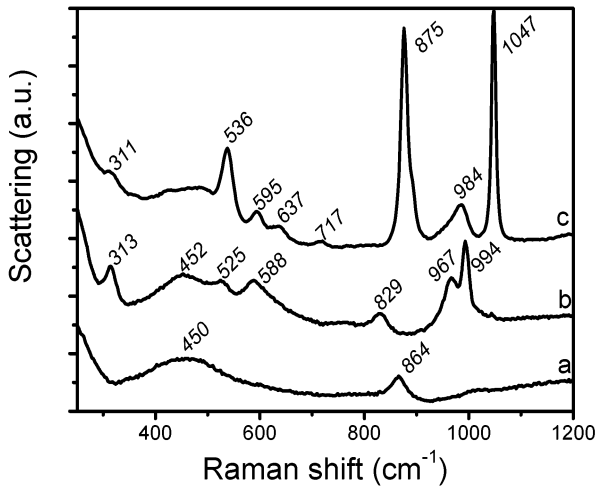

Figure 12. Raman spectra of reference solutions. (a) a monomeric vanadium oxide species VO_4^{3-}; (b) a polymeric vanadium oxide species: $V_{10}O_{26}(OH)_2^{4-}$; and (c) a vanadium oxoperoxo species: $VO(O-O)^+$.

increased with increasing vanadium oxide loading. Furthermore, the area ratio of the 1030/910 cm^{-1} Raman bands has an average value of 1.86 (σ(area ratio) = 0.24) when the vanadium oxide loading increased (Table 1). If the ~900 cm^{-1} Raman band originates from a polymeric V−O−V species, one would expect the Raman band area ratio to decrease with increasing polymerization degree and thus with increasing vanadium oxide loading. Since this is not the case, one has to conclude that the ~900 cm^{-1} band cannot originate from a polymeric species.

Second, Griffith et al. showed that the V−O−V stretch vibration lies below 850 cm^{-1} for polymeric and dimeric vanadium oxide species.[49] The spectrum of aqueous $V_{10}O_{26}(OH)_2$,$^{4-}$ shown in Figure 12b, also indicates that the V−O−V vibrations are not observed above 900 cm^{-1}. Three V−O−V vibrations can be expected in the spectrum of a polymeric species, none of these are expected to be observed above 900 cm^{-1}. The V−O−V bending vibrations are usually observed around 200−300 cm^{-1},[46]and the symmetric and asymmetric stretch vibrations are normally observed between 450 and 900 cm^{-1} (see the Supporting Information). Furthermore, when we combine the V−O single bond distance obtained from EXAFS with the V−O frequency correlation equation from Hardcastle et al., the V−O vibration is expected to be observed around 780 cm^{-1}, which was not the case. It has to be noted that the V═O vibration calculated in the same way mimics the experimentally observed value. Although Hardcastle et al. use the diatomic approximation for their calculation, the reference structures with a V−O bond of ~1.72 Å presented by these authors show that the V−O stretch as well as the symmetry related (V−O−V type) vibrations lie below 900 cm^{-1}. Furthermore, we have observed a similar Raman band around 920 cm^{-1} for 1 wt % V_2O_5 supported on SiO_2,[61] for which polymeric species are never observed.[12,60] Although SiO_2 exhibits a band at 970 cm^{-1}, there is no band from silica observable near 920 cm^{-1}. This finding puts further doubt on the assignment of the 900 cm^{-1} Raman band to a V−O−V vibration.

Also at the lowest loading used in this study, the presence of polymeric species is very unlikely. The absence of polymeric species is also supported by the theoretical monolayer model as described for monomeric and polymeric species by Khodakov et al.[1] The UV−vis−NIR DRS, ESR, and XANES point in the direction of an isolated VO_4 species with the vanadium in the 5+ oxidation state. Taking into account all of these arguments,

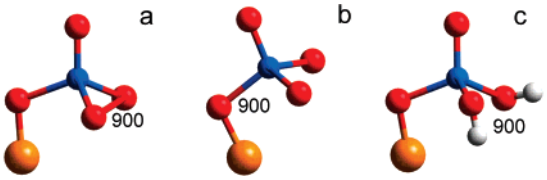

Figure 13. Schematic representation of the alternative assignments for the 900 cm^{-1} vibration.

we believe that the assignment of the 900−920 cm^{-1} Raman band to polymeric vanadium oxide species as is normally done in the literature is incorrect and that the detection of the ~900 cm^{-1} vibration is indicative for the presence of an isolated VO_4 species as well. In what follows, we will put forward potential assignments for this Raman band on the basis of our new supported vanadium oxide model.

Alternative Assignments for the 900−920 cm^{-1} Raman Band. If the umbrella model is indeed true, it leaves room for several alternative assignments of the 900 cm^{-1} Raman band. It is remarkable to notice that the different options have been mentioned in the literature before,[62] with the exception of the vanadium peroxo species. This latter possibility has only been recently introduced by Gijzeman et al.[48] The different options, i.e., a V−O−Al, V−OH, and V−(O−O) vibration, are schematically depicted in Figure 13. In this respect, it is fair to refer to the initial Raman work of the group of Wachs in the early 90s.[16,46,62] These authors indicated that V−OH, V−O−V, and V−O-support vibrations could be located in the region 900−950 cm^{-1} of the Raman spectra. It is remarkable that later on in the literature only the assignment of the V−O−V vibration survived and has been commonly used in the field for structural characterization. This is especially surprising taking into account the experimental evidence that V−O−V vibrations are not located above 900 cm^{-1} in solid compounds as well as in solutions.[46,49]

We will discuss here the pros and cons of the alternative assignments, without making a definite conclusion. Future characterization studies, together with detailed theoretical calculations on realistic molecular models, hopefully will make one of these assignments unambiguous.

A. V−(O−O) Vibration. The first possibility is a perturbed O−O stretch vibration of a peroxo group attached to the central vanadium atom. Gijzeman et al. showed via theoretical calculations on an alumina supported system that the ~900 cm^{-1} band can be assigned to the stretching vibration of a peroxo O−O species for an isolated VO_4 species with one V═O and one V−O support bond.[48] The DFT calculations by Gijzeman et al. have also demonstrated that a peroxo species is capable of explaining the isotopic labeling behavior of vanadium oxide catalysts. An argument pro this assignment is that vibrations of vanadium peroxo species in solutions and solids are generally known to be located in the 900 cm^{-1} region, as is shown in the spectrum of $VO(O-O)^+$ (Figure 12a). However, one has to be aware that vanadium peroxo species are thermally unstable and crystalline vanadium peroxo species dissociate between 473 and 573 K.[63] To verify this optional assignment, the stability of an impregnated vanadium peroxo species on Al_2O_3 was checked and the typical peroxo vibration (ν(O−O)) at 875 cm^{-1} disappeared after drying at 120 °C for one night. One could argue, however, that such peroxo species would be still present, although with altered vibrational frequencies due to the anchoring to the support.

B. V−O−Al Vibration. Magg et al. assigned the 900 cm^{-1} to V−O−Al vibrations on the basis of DFT calculations and $AlVO_4$ reference species.[47,64] They clearly demonstrated that

one could expect a V−O-support vibration in the 900 cm^{-1} region. However, the comparison between their Raman and IR data shows that for these two techniques the peak position is not the same, i.e., 915 cm^{-1} for Raman vs 941 cm^{-1} for IR. Although the measurements were carried out on different samples, we cannot conclude for sure that the band observed in IR originates from the same vibration as the band observed in Raman. It is also possible that the V−O-support vibration is not observable with Raman, since Rice and Scott do not observe the V−O−Si (900 cm^{-1}) Raman band for a $VOCl_3$ compound supported on SiO_2 and Magg et al. do not show data that are conclusive on this point.[47,57,64,65]

On the other hand, Rice and Scott do not have another option for the 900 cm^{-1} vibration than V−O−Si, since their experiments are carried out on a vanadium species which has one V═O bond, two V−Cl bonds, and one V−O−Si bond (Si−O−$VOCl_2$).[58] Although they observe a vibration at higher wavenumber (960 cm^{-1}), which is assigned to the V−O−Si vibration, the Cl atoms might be held accountable for a frequency shift with respect to the data presented in this paper (900−920 cm^{-1}) and by Magg et al. (915 cm^{-1}).[47,64,65] However, one has to realize that with iso-propoxide (O^iPr) or *tert*-butoxide (O^tBu) instead of Cl, the 960 cm^{-1} vibration only shifts by 2 cm^{-1}.[56,57]

Furthermore, we have compared Raman and IR data of SiO_2 supported vanadium oxide catalysts. Both spectroscopic measurements were performed on the same set of catalysts after similar treatments. The vibration frequencies observed in the region 900−1000 cm^{-1} were ∼920 cm^{-1} for Raman and ∼960 cm^{-1} for IR.[61] This observation indicates that there are two different vibrations: one more IR active and the other more Raman active. The interpretation of the 960 cm^{-1} IR band can be indeed the V−O-support vibration, leaving room for another interpretation of the 920 cm^{-1} Raman band.

C. V−O−H Vibration. It is difficult to assign the V−O stretching and the V−O−H bending vibration to specific bands in the IR and Raman spectra. Accurate literature data are lacking, and it should be noted that both vibrations are slightly mixed; displacement of the oxygen atom occurs in both vibrations and thus both modes will affect each other. However, Hirata et al. and Dickens et al. claim that the V−O−H bending vibration appears around 920 cm^{-1} in the IR spectrum of hydrogen inserted vanadium oxide compounds. [66,67]

In general, the X−O−H bending vibration is found at 100−400 cm^{-1} higher wavenumber than the corresponding X−O stretching mode, e.g., 1350 and 1050 cm^{-1} respectively, for C−O−H in a primary alcohol and 1060−1020 cm^{-1} and 955−820 cm^{-1} respectively, for Si−O−H.[68] Regarding the calculated position of the V−O stretch vibration for a V−O bond of 1.72 Å at 788 cm^{-1},[46] assignment of the V−O−H bending to a peak at 900 cm^{-1} is therefore possible. In general the IR peak intensity can be used to confirm an assignment, since the X−O stretching vibrations are usually characterized as "strong" whereas the bending vibrations get the predicate "weak − medium". It implies that a relatively more intense band should be present in the 595−450 cm^{-1} range of the IR spectrum. However, the support materials such as SiO_2 and Al_2O_3 are IR opaque in the X−O stretch region,[18] and for that reason the V−O stretch, although strong, is not observed in the IR spectrum. The thermal stability of the V−OH bond is difficult to assess. The hydrogen inserted vanadium oxide compound loses H as water molecules, and thus the OH vibration, between 50 and 350 °C.[67] However, no definite conclusions can be drawn on the stability of supported V−OH groups at present.

Conclusions

The following conclusions can be drawn from this work:

1. The current V−O−V assignment of the 900 cm^{-1} Raman band in supported vanadium oxide catalysts is incorrect since it is observed in catalysts, which do not contain any V−O−V moieties.

2. EXAFS on a 1 wt % VO_4/Al_2O_3 catalyst under dehydrated conditions revealed the presence of one V═O bond of 1.58 Å and three V−O bonds of 1.72 Å. Knowing the exact coordination number and distance of the support atoms to the vanadium atom led to a new perspective on the isolated supported vanadium oxide species. This model literally turns the vanadium oxide upside down: one V−O-support bond, one V═O bond, and two V−O bonds. EXAFS, however, does not reveal more information about the two latter bonds. It only shows the presence of atoms relative to the central vanadium atom and does not give information on interactions between other atoms, e.g., a O−O bond for a vanadium peroxo species, neither does it show the presence of hydrogen atoms.

3. This new molecular structure has led to three possible assignments of the 900 cm^{-1} band. More specifically, the Raman band can originate from a V−O−Al, a V−O−H, or a V−(O−O) vibration.

This work shows that one must be very careful in making firm assignments of Raman bands in the field of supported metal oxide catalysts. Future work will be focused on isotopic labeling experiments in which Raman and infrared spectroscopy are combined. To further support the above presented conclusions, an extension to other supported vanadium oxide catalysts, such as V/SiO_2, is under way. Finally, obtaining more information on the exact structure of the interface between the catalytically active metal oxide and the support leads to the determination of the influence of the support on the catalytic properties of the supported vanadium oxide catalyst.

Acknowledgment. The work at HASYLAB was supported by the IHP Contract HPRI-CI-2001-00140 of the European Commission. B.M.W acknowledges financial support from NRSCC, NWO/CW-Van der Leeuw, NWO/CW-VICI, CONCORDE, and a EU-COST D15 program. The authors thank Onno Gijzeman, Joost van Lingen, Joop van Lenthe, and Tom Visser (Utrecht University) for useful discussions.

Supporting Information Available: Difference files for raw $O_{(1)}-O_{(2)}$ and $O_{(3)} + V_{(4)} + O_{(5)}$ from EXAFS of 1V−Al for model II (with V-V scatterer pair), together with the magnitude and the imaginary part of the Fourier transform for the separate shells: $O_{(3)}$, $V_{(4)}$, and $O_{(5)}$. Tentative assignments for the Raman bands in the reference spectra of VO_4^{3-}, $V_{10}O_{26}(OH)_2^{4-}$, and $VO(O-O)^+$. This material is available free of charge via the Internet at http://pubs.acs.org.

References and Notes

(1) Khodakov, A.; Olthof, B.; Bell, A. T.; Iglesia, E. *J. Catal.* **1999**, *181*, 205.
(2) Deo, G.; Wachs, I. E. *J. Catal.* **1994**, *146*, 323.
(3) Gao, X.; Fierro, J. L. G.; Wachs, I. E. *Langmuir* **1999**, *15*, 3169.
(4) Haber, J.; Nowak, P.; Serwicka, E. M.; Wachs, I. E. *Bull. Pol. Acad. Sci.* **2000**, *48*, 337.
(5) Wong, G. S.; Kragten, D. D.; Vohs, J. M. *J. Phys. Chem. B* **2001**, *105*.
(6) Bañares, M. A. *Catal. Today* **1999**, *51*, 319.
(7) Martra, G.; Arena, F.; Coluccia, S.; Frusteri, F.; Parmaliana, A. *Catal. Today* **2000**, *63*, 197.
(8) Arena, F.; Frusteri, F.; Parmaliana, A. *Catal. Lett.* **1999**, *60*, 59.
(9) Le Bars, J.; Auroux, A.; Forissier, M.; Vedrine, J. C. *J. Catal.* **1996**, *162*, 250.

(10) Olthof, B.; Khodakov, A.; Bell, A. T.; Iglesia, E. *J. Phys. Chem. B* **2000**, *104*, 1516.
(11) Weckhuysen, B. M.; Keller, D. E. *Catal. Today* **2003**, *78*, 25.
(12) Gao, X.; Bare, S. R.; Weckhuysen, B. M.; Wachs, I. E. *J. Phys. Chem. B* **1998**, *102*, 10842.
(13) Bond, G. C.; Flamerz-Tahir, S. *Appl. Catal.* **1991**, *71*, 1.
(14) Ruitenbeek, M.; van Dillen, A. J.; de Groot, F. M. F.; Wachs, I. E.; Geus, J. W.; Koningsberger, D. C. *Top. Catal.* **2000**, *10*, 241.
(15) Gao, X.; Wachs, I. E. *J. Phys. Chem. B* **2000**, *104*, 1261.
(16) Vuurman, M. A.; Wachs, I. E. *J. Phys. Chem.* **1992**, *96*, 5008.
(17) Van Der Voort, P.; White, M. G.; Mitchell, M. B.; Verberckmoes, A. A.; Vansant, E. F. *Spectrochim. Act. A* **1997**, *53*, 2181.
(18) Wachs, I. E. *Catal. Today* **1996**, *27*, 437.
(19) Takenaka, S.; Tanaka, T.; Yamazaki, T.; Funabiki, T.; Yoshida, S. *J. Phys. Chem. B* **1997**, *101*, 9035.
(20) S. T.Oyama; Went, G. T.; Lewis, K. B.; Bell, A. T.; Somorjai, G. A. *J. Phys. Chem.* **1989**, *93*, 6786.
(21) Eckert, H.; Wachs, I. E. *J. Phys. Chem.* **1989**, *93*, 6796.
(22) Le Coustumer, L. R.; Taouk, B.; Le Meur, M.; Payen, E.; Guelton, M.; Grimblot, J. *J. Phys. Chem.* **1988**, *92*, 1230.
(23) Anpo, M.; Higashimoto, S.; Matsuoka, M.; Zhanpeisov, N.; Shioya, Y.; Dzwigaj, S.; Che, M. *Catal. Today* **2003**, *78*, 211.
(24) Kozlowski, R.; Pettifer, R. F.; Thomas, J. M. *J. Phys. Chem.* **1983**, *87*, 5172.
(25) Bond, G. C.; Perez Zurita, J.; Flamerz, S.; Gellings, P. J.; Bosch, H.; Ommen, J. G. v.; Kip, B. J. *Appl. Catal.* **1986**, *22*, 361.
(26) Went, G. T.; Oyama, S. T.; Bell, A. T. *J. Phys. Chem.* **1990**, *94*, 4240.
(27) Anpo, M.; Sunamoto, M.; Che, M. *J. Phys. Chem.* **1989**, *93*, 1187.
(28) Zhang, S. G.; Higashimoto, S.; Yashimata, H.; Anpo, M. *J. Phys. Chem. B* **1998**, *102*, 5590.
(29) Lin, H.-M.; Kao, S.-T.; Lin, K.-M.; Chang, J.-R.; Shyu, S.-G. *J. Catal.* **2004**, *224*, 156.
(30) López Nieto, J. M.; Kremenic, G.; Fierro, J. L. G. *Appl. Catal.* **1990**, *61*, 235.
(31) Weckhuysen, B. M.; Schoonheydt, R. A. *Catal. Today* **1999**, *49*, 441.
(32) Baes, C. F., Jr.; Mesmer, R. E. *The hydrolysis of cations*; John Wiley & Sons: New York, 1976; p 210.
(33) Kantcheva, M. *Solid State Ionics* **2001**, *141*−*142*, 487.
(34) Delgass, W. N.; Haller, G. L.; Kellerman, R.; Lunsford, J. H. *Spectroscopy in Heterogeneous Catalysts*; Academic Press: New York, 1979.
(35) Kampers, F. W. H.; Maas, T. M. J.; Grondelle, J. v.; Brinkgreve, P.; Koningsberger, D. C. *Rev. Sci. Instrum.* **1989**, *60*, 2635.
(36) Vaarkamp, M., Linders, J. C., Koningsberger, D. C. *Physica B* **1995**, *208/209*, 159.
(37) Koningsberger, D. C.; Mojet, B. L.; Dorssen, G. E. v.; Ramaker, D. E. *Top. Catal.* **2000**, *10*, 143.
(38) Stern, E. A. *Phys. Rev. B* **1993**, *48*, 9825.
(39) Ankudinov, A. L.; Ravel, B.; Rehr, J. J.; Conradson, S. D. *Phys. Rev. B* **1998**, *58*, 7565.
(40) Mustre de Leon, J.; Rehr, J. J.; Zabinski, S. I.; Albers, R. C. *Phys. Rev. B* **1991**, *44*, 4146.
(41) Tillmanns, E.; Baur, W. H. *Acta Crystallogr. B* **1971**, *B27*, 2124.
(42) Hedin, L.; Lundqvist, S. *Solid State Phys.* **1969**.
(43) CERIUS 2; 3.5 ed.; Molecular Simulations Inc.: San Diego, CA, 1997.
(44) Zhou, R.-S.; Snyder, R. L. *Acta Crystallogr.* **1991**, *B47*, 617.
(45) Stobbe-Kreemers, A. W.; Leerdam, G. C. v.; Jacobs, J.-P.; Brongersma, H. H.; Scholten, J. J. F. *J. Catal.* **1995**, *152*, 130.
(46) Hardcastle, F. D.; Wachs, I. E. *J. Phys. Chem.* **1991**, *95*, 5031.
(47) Magg, N.; Immaraporn, B.; Giorgi, J. B.; Schroeder, T.; Baumer, M.; Dobler, J.; Wu, Z.; Kondratenko, E.; Cherian, M.; Baerns, M.; Stair, P. C.; Sauer, J.; Freund, H.-J. *J. Catal.* **2004**, *226*, 88.
(48) Gijzeman, O. L. J.; Lingen, J. N. J. v.; Lenthe, J. H. V.; Tinnemans, S. J.; Keller, D. E.; Weckhuysen, B. M. *Chem. Phys. Lett.* **2004**, *397*, 277.
(49) Griffith, W. P.; Wickins, T. D. *J. Chem. Soc. (A)* **1966**, 1087.
(50) Griffith, W. P.; Wickins, T. D. *J. Chem. Soc. (A)* **1967**, 675.
(51) Griffith, W. P. *J. Chem. Soc. (A)* **1967**, 905.
(52) Dyer, C.; Hendra, P. J.; Forsling, W.; Ranheimer, M. *Spectrochim. Act.* **1993**, *49A*, 691.
(53) Wong, J.; Lytle, F. W.; Messmer, R. P.; Maylotte, D. H. *Phys. Rev. B* **1984**, *30*, 5596.
(54) Tromp, M.; van Bokhoven, J. A.; Arink, A. M.; Bitter, J. H.; van Koten, G.; Koningsberger, D. C. *Chem. Eur. J.* **2002**, *8*, 5667.
(55) Tromp, M.; van Bokhoven, J. A.; van Haaren, R. J.; van Strijdonck, G. P. F.; van der Eerden, A. M. J.; van Leeuwen, P. W. N. M.; Koningsberger, D. C. *J. Am. Chem. Soc.* **2002**, *124*, 14814.
(56) Rice, G. L.; Scott, S. L. *J. Mol. Catal. A: Chem.* **1997**, *125*, 73.
(57) Rice, G. L.; Scott, S. L. *Langmuir* **1997**, *13*, 1545.
(58) Deguns, E. W.; Taha, Z.; Meitzner, G. D.; Scott, S. L. *J. Phys. Chem. B* **2005**, *109*, 5005.
(59) Zheng, X.; Fu, W.; Albin, S.; Wise, K. L.; Javey, A.; Cooper, J. B. *Appl. Spectrosc.* **2001**, *55*, 382.
(60) Burcham, L. J.; Deo, G.; Gao, X.; Wachs, I. E. *Top. Catal.* **2000**, *11/12*, 85.
(61) Keller, D. E.; van Lingen, J. N. J.; Gijzeman, O. L. J.; Koningsberger, D. C.; van Lenthe, J. H.; Weckhuysen, B. M., submitted.
(62) Vuurman, M. A.; Wachs, I. E.; Hirt, A. M. *J. Phys. Chem.* **1991**, *95*, 9928.
(63) Joniaková, D.; Schwendt, P. *Thermochim. Acta* **1985**, *92*, 701.
(64) Magg, N.; Giorgi, J. B.; Schroeder, T.; Bäumer, M.; Freund, H.-J. *J. Phys. Chem. B* **2002**, *106*, 8756.
(65) Magg, N.; Giorgi, J. B.; Hammoudeh, A.; Schroeder, T.; Bäumer, M.; Freund, H.-J. *J. Phys. Chem. B* **2003**, *107*, 9003.
(66) Dickens, P. G.; Chippindale, A. M.; Hibble, S. J.; Lancaster, P. *Mater. Res. Bull.* **1984**, *19*, 319.
(67) Hirata, T.; Yagisawa, K. *J. Alloys Compd.* **1992**, *185*.
(68) Socrates, G. *Infrared Characteristic Group Frequencies*; John Wiley & Sons: Chichester, U.K., 1994.
(69) Campbell, N. J.; Dengel, A. C.; Griffith, W. P. *Polyhedron* **1989**, *8*, 1379.
(70) Fontenot, C. J.; Wiench, J. W.; Pruski, M.; Schrader, G. L. *J. Phys. Chem. B* **2000**, *104*, 11622.